Radiation Physics and Chemistry 175 (2020) 108129

Contents lists available at ScienceDirect

Radiation Physics and Chemistry

journal homepage: www.elsevier.com/locate/radphyschem

Polarization dependent X-ray absorption near-edge spectra of boron nitride nanotubes

Peter Krüger[a,b,*], Yuya Maekawa[a], Adam Hitchcock[c], Carla Bittencourt[d]

[a] Graduate School of Science and Engineering, Chiba University, Chiba 263-8522, Japan
[b] Molecular Chirality Research Center, Chiba University, Chiba 263-8522, Japan
[c] Department of Chemistry and Chemical Biology, McMaster University, Hamilton, ON Canada L8S 4M1
[d] Chemistry Interaction Plasma-Surface (ChIPS), University of Mons, B-7000 Mons, Belgium

ARTICLE INFO

Keywords:
Boron nitride
Nanotubes
Scanning transmission x-ray microscopy
Density functional theory

ABSTRACT

We report polarization dependent, scanning transmission X-ray microscopy measurements of individual boron nitride nanotubes (BNNTs) and analyze them by means of first-principles calculations. X-ray absorption near-edge spectra of hexagonal boron-nitride (hBN) are calculated as a function of light polarization and layer stacking and best agreement with recent experimental data is obtained for the commonly assumed AA' stacking. Our experimental BNNT spectra show a pronounced polarization dependence which is qualitatively well reproduced in the calculations. We show that the BNNT has a mixed stacking sequence which may explain some of the differences seen between the hBN and BNNT line shapes.

1. Introduction

Boron nitride (BN) is structurally very similar to carbon, having a sp^3-bonded cubic and a sp^2 bonded hexagonal phase. As in carbon, the hexagonal (graphitic) phase forms the basis of a wealth of low-dimensional structures including monolayers, nanotubes and fullerenes. Contrary to graphite, however, hexagonal BN (hBN) is an insulator with a large band gap of about 6 eV (Rubio et al., 1994). As a consequence, the technological applications of BN nanostructures are largely complementary to those of carbon nanostructures. Boron nitride nanotubes (BNNT) have a much higher heat and oxidation resistance than carbon nanotubes (Liu et al., 2011) and their band gap of 5.5 eV (Blase et al., 1994) makes them an interesting material for light emitting devices. To better understand the structural and electronic properties of BNNT, we have measured the polarization dependent X-ray absorption near-edge spectroscopy (XANES) of single BNNTs with Scanning Transmission X-ray Microscopy (STXM) (Guttmann and Bittencourt, 2015). We compare the spectra with first principles calculations and study the polarization dependence and the effect of layer stacking in hBN and BNNT.

McDougall et al. (McDougall et al., 2014) has reported a XANES study of bulk hBN for various possible stacking configurations. From total energy considerations and the analysis of XANES and electron energy-loss spectra spectra, the AA' stacking (denoted AB in Ref. McDougall et al. (2014)) was found to be most likely. Recently, the polarization dependence of XANES has been measured on single crystal hBN (Henck et al., 2017) and large changes between in-plane and out-of-plane spectra were observed both at the boron and nitrogen K-edges. To the best of our knowledge however, the detailed polarization dependence of hBN has not yet been studied theoretically, and XANES spectra of single BNNT have not been reported so far.

2. Experimental and computational details

Multi-wall BNNT have been synthesized by ball milling and annealing of boron and LiO_2 in NH_3 gas (Li et al., 2013). We have analyzed individual multi-wall BNNTs made of tens or hundreds of hBN layers and tube diameters in the 100 nm range. Their composition was checked with XPS and the morphology by Transmission Electron Microscopy. STXM measurements were performed using the ambient STXM at the soft X-ray spectromicroscopy beamline 10ID1 (SM) at the Canadian Light Source (CLS, Saskatoon, SK, Canada) with monochromated X-rays focused by a Fresnel zone plate (outer zone width of 40 nm) (Kaznatcheev et al., 2007). The X-rays are generated in an Apple-II type elliptically polarizing undulator (EPU), which produces nearly 100% linearly polarized light in the B 1 s and N 1 s energy ranges. The STXM data was analyzed using the aXis2000 software (Hitchcock A.P., 1997. Analysis of X-ray Images and Spectra (aXis2000) software. 〈http://unicorn.mcmaster.ca/aXis2000.html〉.). Further

* Corresponding author at: Graduate School of Science and Engineering, Chiba University, Chiba 263-8522, Japan.
E-mail addresses: pkruger@chiba-u.jp (P. Krüger), aepa2392@chiba-u.jp (Y. Maekawa), aph@mcmaster.ca (A. Hitchcock), Carla.Bittencourt@umons.ac.be (C. Bittencourt).

https://doi.org/10.1016/j.radphyschem.2019.01.014
Received 29 September 2018; Received in revised form 27 December 2018; Accepted 24 January 2019
Available online 25 January 2019
0969-806X/

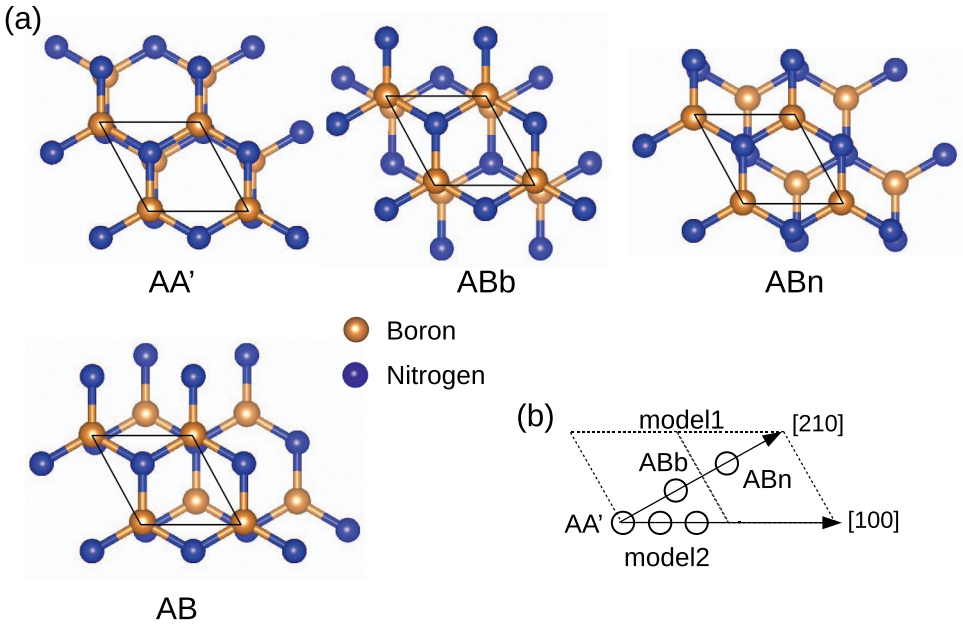

Fig. 1. (a) Stacking configurations of hBN considered in this work. (b) Mixed stacking models for BNNT. Adjacent hBN layers are shifted along [210] or [100] and three shifts are averaged. The shifted position of the lower layer N atom is indicated by a circle.

experimental details will be given in a forthcoming publication.

The calculations have been done using density functional theory (DFT) with the PBE exchange-correlation potential and the projector-augmented wave method as implemented in the VASP code (Kresse and Furthmüller, 1996) with experimental lattice parameters of bulk hBN (a = 2.504 Å, c = 6.661 Å). We set the plane-wave energy cut-off to 400 eV and used 24 × 24 × 8 k-points in the first Brillouin zone of the hBN unit cell. The B and N K-edge XANES are obtained from the unoccupied B-*p* and N-*p* partial density of states (DOS) on the absorber site (Bittencourt et al., 2012; Zhu et al., 2015). In this scheme, the slow energy dependence of the radial transition matrix elements is neglected (de Groot et al., 1993). The DOS is convoluted with a Gaussian of 0.5 eV FWHM to account for experimental broadening and with a Lorentzian of energy-dependent width $\Gamma(E) = \Gamma_c + \Gamma_L(0.5 + \arctan[(E - E_L)/b]/\pi)$ (Bittencourt et al., 2012). We took $\Gamma_L = 0.5$, $b = 3$, $E_L = 12$, $\Gamma_c = 0.05$ (B), $\Gamma_c = 0.1$ (N) (in eV).

The XANES spectra are computed from the final state electronic structure where a core-hole is put on one absorber site in a 4 × 4 × 1 supercell. We use a full core-hole, which gives best agreement with experiment (McDougall et al., 2014). Here the core-hole effect is treated with the final state mode as implemented in VASP (Köhler and Kresse, 2004) (`ICORELEVEL=2`) which includes core-hole screening by valence electrons but neglects screening by other core-electrons. For K-edge spectra of first row elements, this is not a problem, since there are no other core-shells. The core-hole charge is compensated by increasing the number of valence electrons by one. The theoretical spectra are aligned with experiment at threshold. The computed core-level shifts between different stacking configurations are below 0.3 eV and have a negligible effect on the XANES spectra in the mixed stacking models of BN nanotubes. No attempt was made to compute absolute core-level binding energies. For hBN, our spectra are in excellent agreement with calculations using dedicated core-hole pseudopotentials (McDougall et al., 2014; McDougall et al., 2017).

For the present, large BNNTs with a tube diameters of ∼ 100 nm, the curvature of the BN layers is very small on the atomic scale. The bending Δz over the lateral distance Δx of one in-plane lattice constant $a = 2.5$Å, is $\Delta z = a^2/d$ or $\Delta z = 0.6$ pm for $d = 100$ nm. This is below the atomic displacement due to zero-point motion (Allen et al., 2015) and can safely be neglected for the calculation of the electronic structure. Therefore the *local* electronic structure of the multi-wall BNNTs can be well described with calculations on bulk hBN. For the polarization XANES calculation, we perform appropriate averaging over the hBN crystal orientation, in order to account for the cylindrical geometry of the nanotubes. The spectra are obtained from linear combinations of the *p*-projected DOS on the absorber site. In hBN the p_x and p_y-DOS are equal by symmetry. The p_x and p_z-DOS (of either B and N) will be denoted $X(E)$ and $Z(E)$, respectively. Here E is the energy measured from the conduction band minimum, which is identified with the photon energy at the absorption threshold. According to the dipole selection rules of X-ray absorption, the XANES intensity of bulk hBN is then given by Zhu et al. (Zhu et al., 2015),

$$I(\theta, E) \propto X(E)\sin^2\theta + Z(E)\cos^2\theta \,, \tag{1}$$

where θ is the angle between the crystal *c*-axis and the X-ray polarization vector **E**. In the case of BNNTs, we need to average Eq. (1) over the azimuthal angle with respect to the tube axis. This azimuthal average is easily seen to give

$$I(\alpha, E) \propto X(E) + [Z(E) - X(E)]/2 \times \sin^2\alpha \,, \tag{2}$$

where α is the angle between **E** and the tube axis. For the special cases of **E** being parallel or perpendicular to the tube axis, we get

$$I_{\parallel}(E) \propto X(E) \,, \quad I_{\perp}(E) \propto [X(E) + Z(E)]/2 \,. \tag{3}$$

3. Results and discussion

Hexagonal boron nitride. We compare four stacking configurations of hBN: AA', ABb, ABn and AB, see Fig. 1 a. We omit AA stacking, as it has a different out-of-plane lattice constant ($c/2$) and was found unstable (McDougall et al., 2014). According to total energy calculations, stackings AA', ABb and AB stackings have comparable stability, with tiny energy differences of 1 meV (McDougall et al., 2014; Marom et al., 2010). XANES (McDougall et al., 2014) and angle-resolved photoemission experiments (Koch et al., 2018), however, found evidence for AA' stacking. Fig. 2 shows the calculated XANES spectra of hBN in AA' stacking for different polarization angles θ, along with experimental data taken from Henck et al. (Henck et al., 2017). Both B and N spectra display six main features labeled A–F. Peak A originates from the $1s \rightarrow \pi^*$ transition and has strong core-excitonic character (Li et al., 2012). The π^* final states are made of B-p_z and N-p_z orbitals, resulting

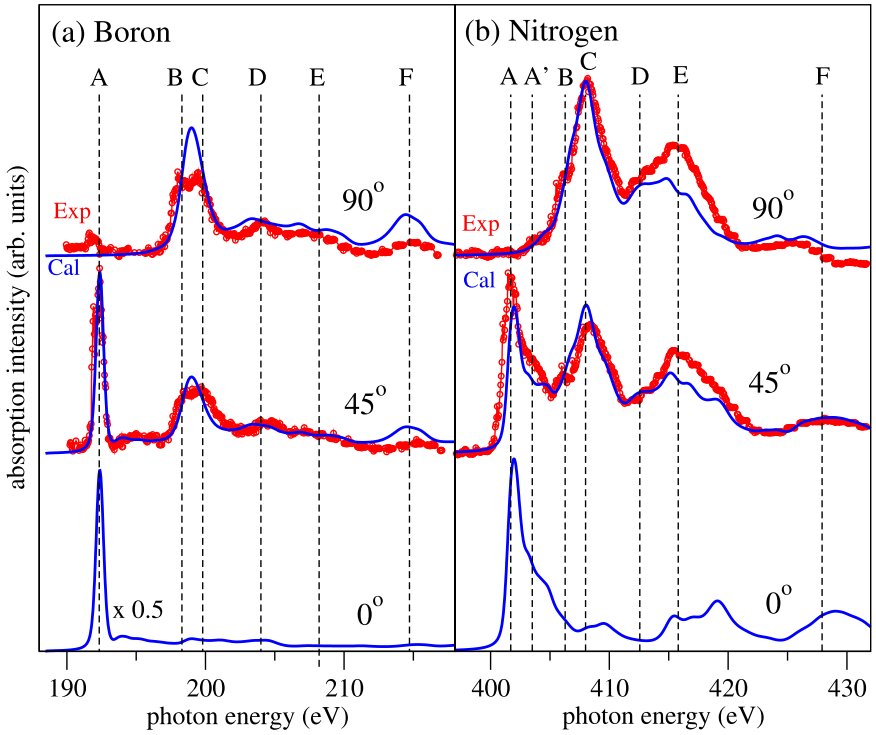

Fig. 2. Polarization dependent XANES spectra of hBN at the (a) boron and (b) nitrogen K-edge. Calculation for AA' stacking (blue lines) vs experimental data taken from Ref. Henck et al. (Henck et al., 2017) (red symbols). The angle θ between polarization vector and surface normal is indicated. In the theoretical spectra, the relative intensity between different polarizations is meaningful. (For interpretation of the references to color in this figure legend, the reader is referred to the web version of this article)

in a $\cos^2\theta$ dependence (Eq. (1)). Peaks B,C have a $\sin^2\theta$ dependence and correspond to the σ^* resonance, i.e. to final states made of B-p_{xy} and N-p_{xy} orbitals. In the N spectra, there is also a shoulder A′ with approximately $\cos^2\theta$ dependence, which has been attributed to interlayer states (Preobrajenski et al., 2004). The spectral region above 415 eV has neither a clear $\cos^2\theta$ nor $\sin^2\theta$ dependence, which indicates that bands of σ and π symmetry overlap. In Fig. 2, the overall agreement between theory and experiment is very good. The most obvious discrepancy is that the B–C peak splitting of about 1.5 eV is missing in the calculated spectra. Note that our non-polarized XANES calculations (not shown) agree very well with those by McDougall et al. (McDougall et al., 2014), who also did not reproduce the B–C splitting in bulk hBN. The same authors recently assigned the splitting to specific lattice defects, namely H-passivated boron vacancies and substitutional carbon at the boron site (McDougall et al., 2017). However, the fact that the splitting is observed quite systematically, in various types of samples (including BNNT) hints to an intrinsic mechanism. It could signal a shortcoming of DFT to describe the excitonic nature of the σ^* resonance (Wang J., Cho, H., Kim, M. J., Sham, T.K., Sun, X., 2015. Nanoscale 7, 1. Layer speciation and electronic structure investigation of freestanding hexagonal boron nitride nanosheets. doi:10.1039/c4nr04445b.).

Since the energy difference between stacking configurations is very small in hBN, other than the AA' configuration may be present as stacking faults. In BNNTs, there is necessarily a mixture of different stackings, due to the curvature of the tubes. Therefore we have also computed the spectra of ABb, ABn and AB. As was found for unpolarized spectra (McDougall et al., 2014) the polarized B K-edge spectra (not shown here) are almost stacking independent. In contrast, the N-spectra, shown in Fig. 3, are quite sensitive to the stacking sequence, especially in the energy range above 410 eV. In Fig. 3, AA' stacking clearly agrees best with experiment, both for $\theta = 90°$ and $\theta = 45°$. Thus our polarization dependent XANES analysis confirms the recent experimental finding that bulk hBN has AA' stacking (McDougall et al., 2014; Henck et al., 2017; Koch et al., 2018).

Boron nitride nanotubes. BNNT are made of rolled up hBN layers. While the local structure can be assumed to be very close to bulk hBN, especially for large multi-wall BNNT considered here, the layer stacking is necessarily different from bulk hBN. Because the circumference between two adjacent layers differs by $\pi c \sim 8a = 20$ Å, the stacking configuration must change continuously when going around the tube, effectively averaging over a gliding direction. Here we consider two simple models (1,2) with gliding directions along [210] and [100], respectively, see Fig. 1 b. The BNNT spectra are modeled by averaging over the shift along the gliding vector. For simplicity we sample the line average with three points in the unit cell. The model 1 spectrum is then just the average of the AA', ABb and ABn spectra. In model 2, two new spectra for the intermediate points were calculated in distorted hBN cells. The spectra are shown in Fig. 4 and compared with experimental data corresponding to single BNNTs lying flat in the image plane with light polarization **E** either parallel or perpendicular to the tube axis. Overall agreement between experiment and theory is good, especially for parallel polarization. The main change brought about in perpendicular polarization, namely the appearance of a large *A* peak is also qualitatively reproduced in the calculation. Thus the present models of BNNT XANES can qualitatively account for the polarization dependent measurements. Quantitatively, however considerable differences between theory and experiment are observed. From Eqs. (1), (3), it is seen that the theoretical BNNT spectra for parallel orientation are identical to the $\theta = 90°$ spectra of hBN, and the perpendicular BNNT spectra are identical to $\theta = 45°$ spectra of hBN. The corresponding experimental spectra in Figs. 2,4 are indeed quite similar, but there are also marked differences. (i) The peaks in the BNNT spectra are less sharp than those of hBN. This may be attributed to the larger degree of structural disorder present in nanotubes as compared to single crystal (hBN) samples. (ii) Peak A of the BNNT perpendicular spectra is much smaller than peak A of hBN (45°), both at the boron and nitrogen edges, indicating that in the BNNT perpendicular spectra, the contribution of $Z(E)$ (π^* states) is considerably less than 50%, at variance with Eq. (3). This

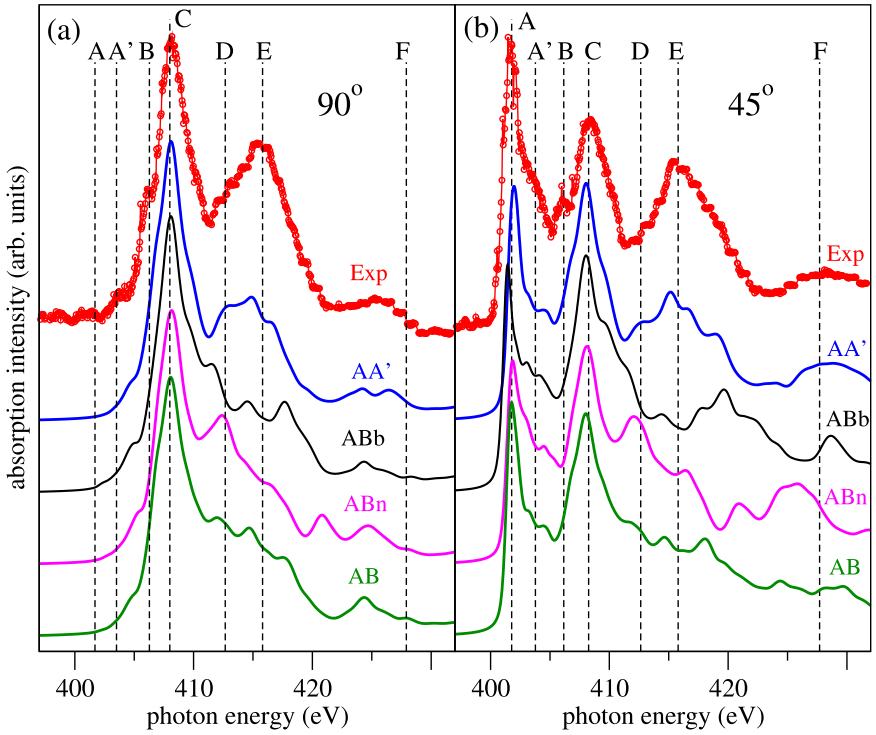

Fig. 3. Calculated nitrogen K-edge XANES spectra (lines) for hBN in different stacking configurations (see Fig. 1) vs experimental data taken from Ref. Henck et al. (2017) (red symbols). (a) Polarization angle $\theta = 90°$. (b) $\theta = 45°$ (For interpretation of the references to color in this figure legend, the reader is referred to the web version of this article).

probably means that our structural model of perfect cylindrical, multi-wall nanotubes is oversimplified. We speculate that in the present, large BNNT, parts of the hBN layers may not be rolled up in perfect cylinders, but exist in different form, possibly similar to BN nano-ribbons. We note that BN nano-ribbons can be formed in a very similar synthesis process (Chen et al., 2006) and often both tubes and ribbons coexist in the sample. In flat-lying nanoribbons, the **E** vector lies in the hBN plane independently of θ and so the spectrum is 100% $X(E)$ whatever the polarization. Therefore, if the BNNTs have partly nanoribbon structure, we expect a decrease of $Z(E)$ signal in perpendicular polarization and a concomitant reduction of the polarization dependence, as observed in the present data. (iii) Another marked difference is that peak D of the N spectrum, which is very weak in hBN, is much stronger in BNNT. Looking at the stacking dependence in Fig. 3, we see that the D-peak is more pronounced for ABn than for AA' stacking. The overall agreement with experiment is comparable between pure AA' stacking and models 1

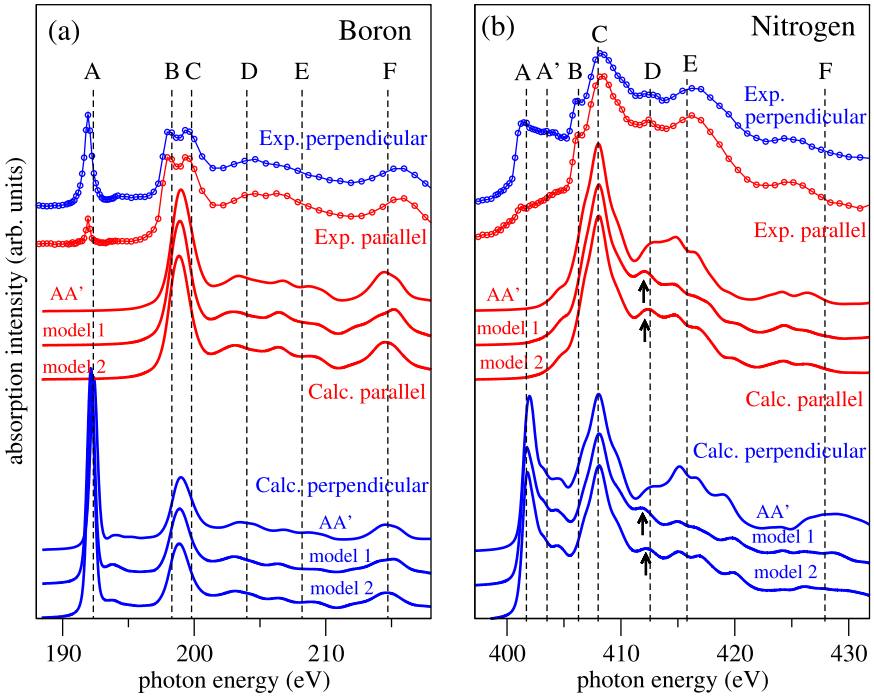

Fig. 4. Experimental (symbols) and calculated (lines) XANES spectra at (a) boron and (b) nitrogen K-edge of BNNT with parallel (red) and perpendicular (blue) polarization. Pure AA' and mixed stackings model 1 and model 2, see Fig. 1 (For interpretation of the references to color in this figure legend, the reader is referred to the web version of this article).

or 2. However, in models 1 and 2, peak D (small arrows in Fig. 4) is relatively enhanced in models 1,2. This fits the enhancement of the peak D in BNNT as compared to hBN and so it is strong evidence that the multi-wall BNNT have a mixed stacking sequence rather than pure AA'.

4. Conclusions

In summary we have studied the polarization dependent XANES of hBN and single BN nanotubes using STXM experiments and first principles modeling. For hBN, we obtain good agreement with recent experimental data, confirming AA' as the most likely stacking configuration. The BNNT spectra display substantial dichroism between light polarized parallel and perpendicular to the tube axis. The polarization dependence is qualitatively reproduced with a model of perfectly cylindrical multi-wall nanotubes, but the measured dichroism is considerably smaller than the calculated one. This indicates that the present, large multi-wall nanotubes have a more complex structure, which may partly resemble BN nanoribbons. For the necessarily mixed layer stacking in the nanotubes, we considered two simple models which help explain some differences between the hBN and nanotube line shapes.

Acknowledgments

Funding by JSPS KAKENHI under Grant no. 16K05393 is gratefully acknowledged.

References

Allen, C.S., Liberti, E., Kim, J.S., Xu, Q., Fan, Y., He, K., Robertson, A.W., Zandbergen, H.W., Warner, J.H., Kirkland, A.I., 2015. Temperature dependence of atomic vibrations in mono-layer graphene. J. Appl. Phys. 118, 074302. https://doi.org/10.1063/1.4928324.

Bittencourt, C., Krüger, P., Lagos, M.J., Ke, X., Van Tendeloo, G., Ewels, C., Umek, P., Guttmann, P., 2012. Towards atomic resolution in sodium titanate nanotubes using near-edge X-ray-absorption fine-structure spectromicroscopy combined with multichannel multiple-scattering calculations. Beilstein J. Nanotechnol. 3, 789–797. https://doi.org/10.3762/bjnano.3.88.

Blase, X., Rubio, A., Louie, S.G., Cohen, M.L., 1994. Stability and band gap constancy of boron nitride nanotubes. Europhys. Lett. 28, 335–340. https://doi.org/10.1209/0295-5075/28/5/007.

Chen, Y., Li, C.P., Chen, H., Chen, Y., 2006. One-dimensional nanomaterials synthesized using high-energy ball milling and annealing process. Sci. Technol. Adv. Mater. 7, 839–846. https://doi.org/10.1016/j.stam.2006.11.014.

de Groot, F.M.F., Faber, J., Michiels, J.J.M., Czyzyk, M.T., Abbate, M., Fuggle, J.C., 1993. Oxygen 1s X-ray absorption of tetravalent titanium oxides: a comparison with single-particle calculations. Phys. Rev. B 48, 2074–2080. https://doi.org/10.1103/PhysRevB.48.2074.

Guttmann, P., Bittencourt, C., 2015. Overview of nanoscale NEXAFS performed with soft X-ray microscopes. Beilstein J. Nanotechnol. 6, 595–604. https://doi.org/10.3762/bjnano.6.61.

Henck, H., Pierucci, D., Aziza, Z.B., Silly, M.G., Gil, B., Sirotti, F., Cassabois, G., Ouerghi, A., 2017. Stacking fault and defects in single domain multilayered hexagonal boron nitride. Appl. Phys. Lett. 110, 023101. https://doi.org/10.1063/1.4972848.

Hitchcock A.P., 1997. Analysis of X-ray Images and Spectra (aXis2000) software. ⟨http://unicorn.mcmaster.ca/aXis2000.html⟩.

Kaznatcheev, K., Karunakaran, C., Lanke, U., Urquhart, S., Obst, M., Hitchcock, A.P., 2007. Soft X-ray spectromicroscopy beamline at the CLS: commissioning results. Nucl. Instrum. Methods Phys. Res., Sect. A 582, 96–99. https://doi.org/10.1016/j.nima.2007.08.083.

Koch, R.J., Katoch, J., Moser, S., Schwarz, D., Kawakami, R.K., Bostwick, A., Rotenberg, E., Jozwiak, C., Ulstrup, S., 2018. Electronic structure of exfoliated and epitaxial hexagonal boron nitride. Phys. Rev. Mater. 2, 074006. https://doi.org/10.1103/PhysRevMaterials.2.074006.

Köhler, L., Kresse, G., 2004. Density functional study of CO on Rh(111). Phys. Rev. B 70, 165405. https://doi.org/10.1103/PhysRevB.70.165405.

Kresse, G., Furthmüller, J., 1996. Efficient iterative schemes for ab initio total-energy calculations using a plane-wave basis set. Phys. Rev. B 54, 11169–11186. https://doi.org/10.1103/PhysRevB.54.11169.

Li, L., Liu, X., Li, L., Chen, Y., 2013. High yield BNNTs synthesis by promotion effect of milling-assisted precursor. Microelectron. Eng. 110, 256–259. https://doi.org/10.1016/j.mee.2013.01.044.

Li, L.H., Petravic, M., Cowie, B.C.C., Tan Xing, T., Peter, R., Chen, Y., Si, C., Duan, W., 2012. High-resolution x-ray absorption studies of core excitons in hexagonal boron nitride. Appl. Phys. Lett. 101, 191604. https://doi.org/10.1063/1.4767135.

Liu, L., Sham, T., Han, W., Zhi, C., Bando, Y., 2011. X-ray excited optical luminescence from hexagonal boron nitride nanotubes: electronic structures and the role of oxygen impurities. ACS Nano 2011 (5), 631–639. https://doi.org/10.1021/nn102881j.

Marom, N., Bernstein, J., Garel, J., Tkatchenko, A., Joselevich, E., Kronik, L., Hod, O., 2010. Stacking and registry effects in layered materials: the case of hexagonal boron nitride. Phys. Rev. Lett. 105, 046801. https://doi.org/10.1103/PhysRevLett.105.046801.

McDougall, N.L., Nicholls, R.J., Partridge, J.G., McCulloch, D.G., 2014. The near edge structure of hexagonal boron nitride. Microsc. Microanal. 20 (1053), 2014. https://doi.org/10.1017/S1431927614000737.

McDougall, N.L., Partridge, J.G., Nicholls, R.J., Russo, S.P., McCulloch, D.G., 2017. Influence of point defects on the near edge structure of hexagonal boron nitride. Phys. Rev. B 96, 144106. https://doi.org/10.1103/PhysRevB.96.144106.

Preobrajenski, A.B., Vinogradov, A.S., Martensson, N., 2004. Ni 3d-BN π hybridization at the h-BN/Ni(111) interface observed with core-level spectroscopies. Phys. Rev. B 70, 165404. https://doi.org/10.1103/PhysRevB.70.165404.

Rubio, A., Corkill, J.L., Cohen, M.L., 1994. Theory of graphitic boron nitride nanotubes. Phys. Rev. B 49 (R), 5081. https://doi.org/10.1103/PhysRevB.49.5081.

Wang J., Cho, H., Kim, M. J., Sham, T.K., Sun, X., 2015. Nanoscale 7, 1. Layer speciation and electronic structure investigation of freestanding hexagonal boron nitride nanosheets. doi:10.1039/c4nr04445b.

Zhu, X., Hitchcock, A., Bittencourt, C., Umek, P., Krüger, P., 2015. Individual titanate nanoribbons studied by 3D-resolved polarization dependent X-ray absorption spectra measured with scanning transmission X-ray microscopy. J. Phys. Chem. C 119, 24192–24200. https://doi.org/10.1021/acs.jpcc.5b08539.